Available online at www.sciencedirect.com
SCIENCE DIRECT®
PHOTONICS AND NANOSTRUCTURES Fundamentals and Applications
Photonics and Nanostructures – Fundamentals and Applications 4 (2006) 132–140
www.elsevier.com/locate/photonics

Suppressing the effect of disorders using time-reversal symmetry breaking in magneto-optical photonic crystals: An illustration with a four-port circulator☆

Zheng Wang *, Shanhui Fan

Edward Ginzton Laboratory, Stanford University, Stanford, CA 94305-4085, USA

Received 15 September 2005; received in revised form 20 January 2006; accepted 4 February 2006
Available online 28 February 2006

Abstract

In integrated optical systems, nonreciprocal elements are indispensable devices that eliminate multi-path reflection between components. To miniaturizing these devices down to a single-wavelength scale, we study nonreciprocal effects in point defects of magneto-optical photonic crystals. The nonreciprocal effect splits degenerate mode pairs and its strength is maximized by spatially matching the magnetic domain pattern with a modal cross product. The resultant eigenmodes are a pair of counter-rotating states that lack time-reversal symmetry. Based upon these eigenmodes, we propose a micro-cavity four-port circulator constructed by coupling a magneto-optical cavity with two waveguides, where each rotating state supports light tunneling along a different direction. In the presence of strong magneto-optical couplings, due to time-reversal symmetry breaking, the performance of the isolator is fundamentally protected from the effect of small structural fluctuations. Numerical calculations demonstrate a four-port circulator with a 26 dB isolation and a roughness tolerance on the order of $0.1a$, where a is the lattice constant of the crystal.

PACS: 42.70.Qs; 42.82.Et; 85.70.Sq

Keywords: Magneto-optics; Photonic crystals; Optical resonances; Channel add/drop filters; Optical circulators; Nonreciprocity

1. Introduction

Photonic crystals have been shown to be a promising platform for creating large-scale optical integrated circuits that are necessary to address the increasing demand of optical information processing for broader communication bandwidth [1–3]. Photonic crystal defect states, in particular, provide a mechanism to systematically miniaturize devices down to a single-wavelength scale. The use of such devices may reduce the production cost and provide greater functionality in large-scale circuits. Among various photonic crystal devices, non-reciprocal optical elements have been intensely researched [4–6]. Non-reciprocal devices, allows light to propagate only along a single direction, and are important for reducing the back scattering, suppressing the laser noise and improving system stability [7]. To create such devices typically requires breaking time-reversal symmetry through the use of magneto-optical materials.

In this paper we focus upon a four-port circulator, constructed by introducing magneto-optical defects into an in-plane four-port channel add/drop filter as

☆ This article is based on a presentation given at the Sixth International Symposium on Photonic and Electromagnetic Crystal Structures (PECS-VI).

* Corresponding author at: 316 Via Pueblo Mall, Department of Applied Physics, Stanford, CA 94305-4090, USA.
Tel.: +1 650 704 2405; fax: +1 650 7257509.
E-mail address: Zheng.Wang@stanford.edu (Z. Wang).

1569-4410/$ – see front matter
doi:10.1016/j.photonics.2006.02.001

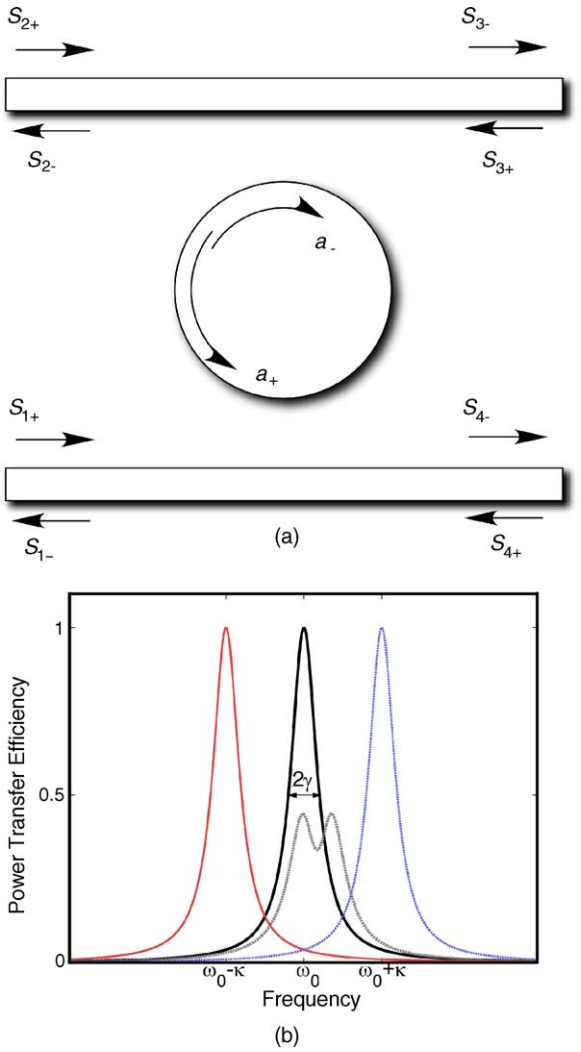

Fig. 1. (a) Schematics of a four-port channel add-drop filter (ADF). The straight arrows indicate the incoming and outgoing waves. The curved arrows represent the two counter-rotating modes in the resonator. (b) Spectra of transfer efficiency of various four-port ADFs. The blank curve represents an ideal ADF resonant at ω_0 with a line-width γ. Such an ADF supports two resonant modes that are degenerate in both frequency and linewidth. The gray dashed line corresponds to a filter structure in which the two modes have the same width γ, and with a frequency split of 1.7γ. The red (blue) curves corresponds to the transfer efficiency from ports 1 to 2 (2 to 1), in the presence of a strong magneto-optical coupling with a coupling strength κ.

first proposed in Ref. [8]. The entire system, as sketched in Fig. 1, consists of a bus waveguide and a drop waveguide, both evanescently coupled to a resonator. For a reciprocal add/drop filter without magneto-optical materials, the optical resonator in the add/drop filter supports two doubly-degenerate counter-rotating modes. On resonance, an optical signal can tunnel from the bus (drop) waveguide to the drop (bus) waveguide through the clockwise (counter-clockwise) rotating state, while off-resonance signals remain in the original waveguide [8,9]. To create a non-reciprocal device, we introduce magneto-optical material into the cavity to create strong magneto-optical coupling of modes inside the cavity. The resulting cavity eigenstates become two circularly rotating modes along opposite directions at different frequencies. The strength of such coupling can be maximized with an appropriate domain design, and is only limited by the gyrotropic coefficients of the magneto-optical materials. With a strong magneto-optical coupling, the frequency splitting between the two resonant modes can be larger than the cavity linewidths that result from cavity-waveguide coupling. In such a case, the device functions as an optical circulator. In order to demonstrate this device in a practical system, we note that one could start with the channel add/drop filters that have been demonstrated in photonic crystal slabs, [10,11] and infiltrate only the cavity region with magneto-optical material. The resulting four-port circulators occupy a footprint on a single micron scale and readily integrate with other planar components.

In addition, many of the effects caused by structural disorders in channel add/drop filters can also be fundamentally suppressed by a strong magneto-optical coupling supported by an optimized domain design. In a reciprocal add/drop filter, the ideal 100% dropping efficiency of a reciprocal structure therefore relies upon two counter-rotating resonances with the same frequency and linewidth. Preserving such degeneracy condition translates to stringent tolerance requirement, and demands strict experimental controls. Small fabrication imperfections, such as sidewall roughness, can split and couple the two resonances into standing wave modes at different frequencies, and result in low transfer efficiency as well as strong reflection back to the input port. In contrast, here we show that, in a non-reciprocal structure, with a strong magneto-optical coupling, the counter-rotating states are spectrally well separated, which significantly reduces detrimental mode mixing caused by disorder-related perturbation. Consequently, the ideal channel add/drop characteristics and circulator operation can sustain regardless of small structural variations.

2. Brief review of the operating principle of a reciprocal channel add/drop filter

We start by briefly reviewing the operating principle of reciprocal channel ADF structures in photonic crystals, highlighting only those features that are

relevant for the discussions of magneto-optical effects. The structure, as illustrated in Fig. 1a, can be analyzed with a coupled-mode approach [12–14]. With a mirror symmetry, a photonic crystal defect supports an even modes $|\mathrm{e}\rangle$ and an odd mode $|\mathrm{o}\rangle$, oscillating at complex frequencies of $\omega_{\mathrm{e,o}} + i2\gamma_{\mathrm{e,o}}$, respectively. The time evolution of the cavity mode amplitudes $a_{\mathrm{e,o}}$ in the presence of the incoming (outgoing) waves at the port i with amplitude $S_{i+(-)}$ are described by the following equations:

$$\frac{\mathrm{d}}{\mathrm{d}t}\begin{pmatrix} a_{\mathrm{e}} \\ a_{\mathrm{o}} \end{pmatrix} = \begin{pmatrix} i\omega_{\mathrm{e}} - 2\gamma_{\mathrm{e}} & 0 \\ 0 & i\omega_{\mathrm{o}} - 2\gamma_{\mathrm{o}} \end{pmatrix}\begin{pmatrix} a_{\mathrm{e}} \\ a_{\mathrm{o}} \end{pmatrix} + \mathbf{K}_{\mathrm{eo}}^{T}\begin{pmatrix} S_{1+} \\ S_{2+} \\ S_{3+} \\ S_{4+} \end{pmatrix}, \tag{1}$$

$$\begin{pmatrix} S_{1-} \\ S_{2-} \\ S_{3-} \\ S_{4-} \end{pmatrix} = \begin{pmatrix} 0 & 0 & 0 & 1 \\ 0 & 0 & 1 & 0 \\ 0 & 1 & 0 & 0 \\ 1 & 0 & 0 & 0 \end{pmatrix}\begin{pmatrix} S_{1+} \\ S_{2+} \\ S_{3+} \\ S_{4+} \end{pmatrix} + \mathbf{D}_{\mathrm{eo}}\begin{pmatrix} a_{\mathrm{e}} \\ a_{\mathrm{o}} \end{pmatrix}. \tag{2}$$

By observing the constraints from energy conservation and time-reversal symmetry, one can show that [14]:

$$\mathbf{K}_{\mathrm{eo}} = \mathbf{D}_{\mathrm{eo}} = \begin{pmatrix} i\sqrt{\gamma_{\mathrm{e}}} & \sqrt{\gamma_{\mathrm{o}}} \\ -i\sqrt{\gamma_{\mathrm{e}}} & \sqrt{\gamma_{\mathrm{o}}} \\ -i\sqrt{\gamma_{\mathrm{e}}} & -\sqrt{\gamma_{\mathrm{o}}} \\ i\sqrt{\gamma_{\mathrm{e}}} & -\sqrt{\gamma_{\mathrm{o}}} \end{pmatrix}. \tag{3}$$

When an accidental degeneracy of the complex frequencies, i.e. $\omega_{\mathrm{e}} = \omega_{\mathrm{o}}$ and $\gamma_{\mathrm{e}} = \gamma_0$, is maintained through a proper cavity design, an input wave from port 1 excites a circularly rotating state $|+\rangle = (|\mathrm{e}\rangle + i|\mathrm{o}\rangle)/\sqrt{2}$. Such a state then decays only into ports 2 and 4. [9] The destructive interference between the decaying wave from the cavity and direct transmission from port 1 to 4 leads to zero transmission at port 4, while the decaying wave at port 2 creates a complete transfer on resonance. The time-reversed transfer from port 2 to port 1 occurs at the same frequency through the other resonant mode $|-\rangle = (|\mathrm{e}\rangle - i|\mathrm{o}\rangle)/\sqrt{2}$.

Mathematically, when the degeneracy condition is satisfied, the operation of the device can be more easily described with Eqs. (4)–(6), which are equivalent to Eqs. (1)–(3) via a unitary transformation:

$$\frac{\mathrm{d}}{\mathrm{d}t}\begin{pmatrix} a_{+} \\ a_{-} \end{pmatrix} = \begin{pmatrix} i\omega_{+} - 2\gamma_{\mathrm{o}} & 0 \\ 0 & i\omega_{-} - 2\gamma_{\mathrm{o}} \end{pmatrix}\begin{pmatrix} a_{+} \\ a_{-} \end{pmatrix} + \mathbf{K}_{\pm}^{T}\begin{pmatrix} S_{1+} \\ S_{2+} \\ S_{3+} \\ S_{4+} \end{pmatrix}, \tag{4}$$

$$\begin{pmatrix} S_{1-} \\ S_{2-} \\ S_{3-} \\ S_{4-} \end{pmatrix} = \begin{pmatrix} 0 & 0 & 0 & 1 \\ 0 & 0 & 1 & 0 \\ 0 & 1 & 0 & 0 \\ 1 & 0 & 0 & 0 \end{pmatrix}\begin{pmatrix} S_{1+} \\ S_{2+} \\ S_{3+} \\ S_{4+} \end{pmatrix} + \mathbf{D}_{\pm}\begin{pmatrix} a_{+} \\ a_{-} \end{pmatrix},$$

$$\mathbf{K}_{\pm} = \sqrt{2\gamma_{\mathrm{o}}}\begin{pmatrix} i & 0 \\ 0 & 1 \\ -i & 0 \\ 0 & -1 \end{pmatrix},$$

$$\mathbf{D}_{\pm} = \sqrt{2\gamma_{\mathrm{o}}}\begin{pmatrix} 0 & 1 \\ -i & 0 \\ 0 & -1 \\ i & 0 \end{pmatrix} \tag{5}$$

$$\omega_{+} = \omega_{-}. \tag{6}$$

Using Eqs. (4)–(6), the spectrum for transmission, transfer and reflection can be determined as

$$\begin{aligned} T_{1\to 2} &= T_{2\to 1} = T_{3\to 4} = T_{4\to 3} \\ &= \left|\frac{2\gamma}{j(\omega-\omega_0)+2\gamma}\right|^2, \\ T_{1\to 4} &= T_{4\to 1} = T_{2\to 3} = T_{3\to 2} \\ &= 1\left|1 - \frac{2\gamma}{j(\omega-\omega_0)+2\gamma}\right|, \\ R_1 &= R_2 = R_3 = R_4 = T_{1\to 3} = T_{3\to 1} \\ &= T_{2\to 4} = T_{4\to 2} = 0. \end{aligned} \tag{7}$$

Thus, complete transfer between the bus and drop waveguides and zero reflection can be achieved on resonance ω_{o} with a bandwidth of 2γ. (Fig. 1b)

In fabricated devices, the dielectric function $\varepsilon_{\mathrm{r}}(\mathbf{r})$ would unavoidably deviate from the designed dielectric function $\varepsilon_{\mathrm{d}}(\mathbf{r})$. The effects of small perturbations, i.e. $\Delta\varepsilon_{\mathrm{r}} = \varepsilon_{\mathrm{r}} - \varepsilon_{\mathrm{d}}$, can be treated by introducing an off-diagonal element [15]:

$$\mathbf{V}_{e,o} = \frac{\omega_o}{2}\int \varepsilon_d^2\left[\frac{1}{\varepsilon_r}-\frac{1}{\varepsilon_d}\right]\vec{E}_e^{\,*}\cdot\vec{E}_o\,dV \tag{8}$$

into the frequency matrices in Eqs. (1) and (4). Here we assume that the disorder in the vicinity of the cavity does not affect significantly the cavity-waveguide coupling. Such perturbation lifts the degeneracy and destroys the preferred eigenstates $|e\rangle \pm i|o\rangle$, resulting in significant reflection and reduction in transfer efficiency. As an example, we show in Fig. 1b the spectrum of transfer efficiency, assuming that the two resonances have the same decay rate, but are separated in real part of the frequency by 1.7γ. In general, the spectrum deviates significantly from ideal characteristics when the frequency splitting is comparable to the width of the resonance. Since the quality factor of these structures is typically greater than 1000, as dictated by the channel spacing in WDM systems, [7] the resulting requirements for fabrication accuracy can be very stringent.

3. A four-port optical circulator with magneto-optical materials in the cavity

Here we seek to design an optical circulator with nonreciprocal transmission properties based upon the add/drop filter discussed in the previous section. It was recently shown that when magneto-optical material is introduced into the cavity region, the resulting eigenstates can assume a circularly "hybridized" waveform $|e\rangle \pm i|o\rangle$ [16]. In this case, the time-reversal symmetry is broken, and the counter-rotating mode pair $|e\rangle \pm i|o\rangle$ (a time-reversed image of each other in regular dielectric systems) oscillates at different frequencies.

Analytically, the effect due to the presence of magneto-optical materials can be described with imaginary and anti-symmetric off-diagonal elements in the frequency matrix [17]. In the case of two modes, if we start with a structure that satisfies the degeneracy condition, after the introduction of magneto-optical effects, Eq. (1) is modified as:

$$\frac{d}{dt}\begin{pmatrix} a_e \\ a_o \end{pmatrix} = \begin{pmatrix} i\omega_o - 2\gamma_o & i\kappa \\ -i\kappa & i\omega_o - 2\gamma_o \end{pmatrix}\begin{pmatrix} a_e \\ a_o \end{pmatrix} + \mathbf{K}_{eo}^{T}\begin{pmatrix} S_{1+} \\ S_{2+} \\ S_{3+} \\ S_{4+} \end{pmatrix}. \tag{9}$$

Diagonalizing the frequency matrix yields equations that are the same as Eqs. (4) and (5), except with $\omega_+ = \omega_0 + \kappa$ and $\omega_- = \omega_0 - \kappa$. The transmission, reflection, and transfer spectra can be calculated from Eqs. (5) and (9) as

$$\begin{aligned} T_{1\to2} &= T_{3\to4} = \left|\frac{2\gamma}{j(\omega-\omega_+)+2\gamma}\right|^2, \\ T_{2\to1} &= T_{4\to3} = \left|\frac{2\gamma}{j(\omega-\omega_-)+2\gamma}\right|, \\ T_{1\to4} &= T_{3\to2} = \left|1-\frac{2\gamma}{j(\omega-\omega_+)2\gamma}\right|^2, \\ T_{2\to3} &= T_{4\to1} = \left|1-\frac{2\gamma}{j(\omega-\omega_-)+2\gamma}\right|^2. \end{aligned} \tag{10}$$

Thus, ideal channel add/drop characteristics are maintained, while the transport properties become direction-dependent and nonreciprocal. Under the condition of $|\omega_+ - \omega_-| \gg \gamma$, the backward transmission at the resonance frequency of the forward resonance is much less than unity, as $T_{2\to1}$=$T_{4\to3} \ll 1$. The system functions as a four-port circulator: $T_{1\to2} = T_{2\to3} = T_{3\to4} = T_{4\to1} = T_{2\to1} = T_{3\to2} = T_{4\to3} = T_{1\to4} \sim 0$.

When the frequency separation induced by magneto-optics is much larger than the splitting caused by fabrication disorders, the eigenstates of the systems are largely immune from fabrication disorders. The presence of disorders introduces additional *real* off-diagonal elements (i.e. $\mathbf{V}_{e,o}$ as defined in Eq. (8)) into the frequency matrix. However, $|e\rangle \pm i|o\rangle$ remain the eigenstates of the matrix in Eq. (9), as long as magneto-optical coupling dominates, i.e. $|\kappa| \gg |\mathbf{v}_{eo}|$. Consequently, the ideal operation of the ADF is protected against disorders when significant magneto-optical coupling is present.

4. Simulations of a four-port circulator

We now present a concrete example of an optical circulator constructed from a photonic crystal ADF incorporating magneto-optical materials. (Fig. 2) The crystal consists of a triangular lattice of air holes in bismuth iron garnet (BIG) with $\varepsilon_\perp = 6.25$, and possesses a bandgap for TE modes that have their magnetic field polarized normal to the plane. The air holes have a radius of $0.35a$, where a is the lattice constant. A point defect is created by replacing an air hole with an air ring with an inner radius of $0.55a$ and an outer radius of $1.1a$. Because of the six-fold rotational symmetry, the point defect can support doubly degenerate TE quadrupole modes at $\omega = 0.3400(2\pi c/a)$. The two modes are distinguished by the spatial symmetry of the magnetic fields with respect to both the vertical axis and the

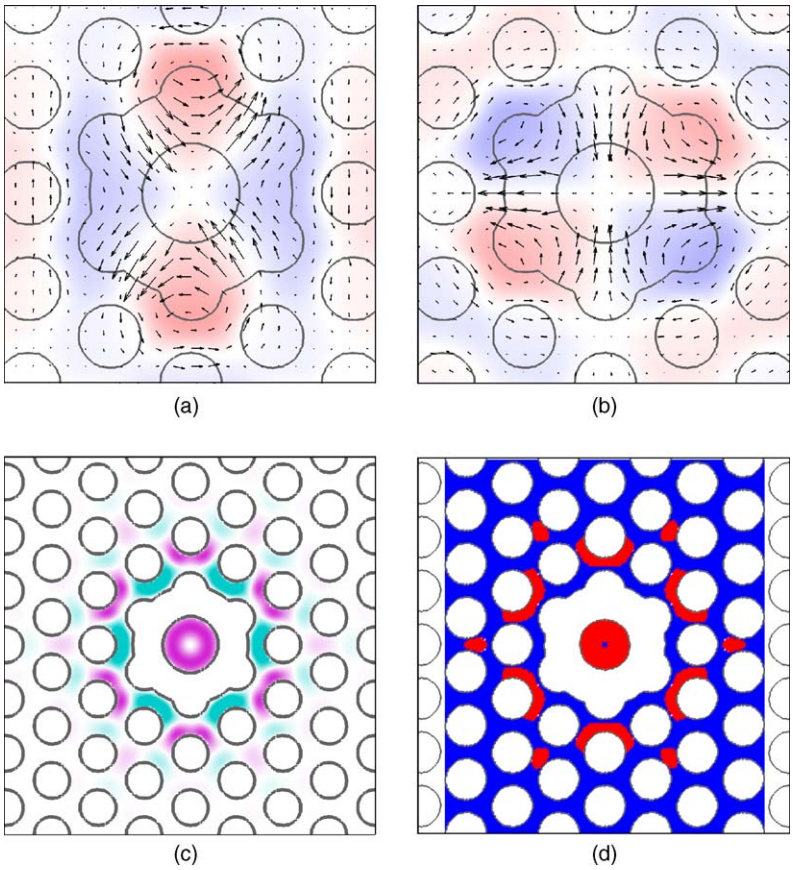

Fig. 2. A defect structure in a photonic crystal. The crystal consists of a triangular lattice of air holes with a radius of $0.35a$, introduced in a dielectric of $\varepsilon = 6.25$ (bismuth iron garnet). The defect is created by replacing an air hole with an air ring of an inner radius of $0.55a$ and an outer radius of $1.1a$. The colored images represent the H_z field distribution of the two doubly-degenerate quadrupole modes, with an even symmetry (a) and an odd symmetry (b) with respect to the vertical center line. The calculation is performed using a plane-wave expansion method. [29] The corresponding electric fields are illustrated with the vector plots. (c) The cross-product between the electric fields of the even and the odd modes. (d) The corresponding domain pattern that maximizes the magneto-optical coupling constant. The blue and red (magenta and cyan) regions denote large positive and negative fields along out of plane directions.

horizontal axis of the cavity. The field distributions of the even mode $|\mathrm{e}\rangle$ and the odd mode $|\mathrm{o}\rangle$ are shown in Fig. 2a and b, respectively.

To create an ADF we introduce two waveguides that couple to the point defect. (Fig. 3, inset) The waveguides consist of line defects of enlarged air holes with a radius of $0.55a$, and are placed six rows away from the cavity. In the presence of the waveguide, the rotational symmetry of the structure is broken and hence the degeneracy between the even and odd modes is lifted. We restore the degeneracy in terms of both the frequency and the quality factor by modifying four air holes at the inner side of the waveguides next to the symmetric axis with slightly reduced radii of $0.33a$. For this structure, we simulate its response function with two-dimensional finite-difference time-domain simulations. The calculated transfer spectrum exhibits a Lorentzian peak with 100% efficiency and a linewidth of $4.43 \times 10^{-5}(2\pi c/a)$, corresponding to a quality factor of 7671. Since there is no magneto-optical effect applied, the transfer spectra in forward and backward directions are identical and therefore reciprocal, as described by the coupled-mode theory.

In the presence of magneto-optical materials inside the cavity, the even and odd modes are no longer eigenmodes of the system. Rather, they couple with a coupling strength:[17]

$$\mathbf{V} = i\kappa_{\mathrm{eo}} = \frac{i}{2}\sqrt{\omega_{\mathrm{e}}\omega_{\mathrm{o}}}\int \varepsilon_{\mathrm{a}}\hat{z}\cdot(\vec{E}_{\mathrm{e}}^{\,*}\times\vec{E}_{\mathrm{o}})\mathrm{d}V, \tag{11}$$

where $\vec{E}_e$ and $\vec{E}_o$ are electric fields of the even mode and the odd mode respectively, and ε_{a} is the off-diagonal gyrotropic element in the dielectric tensor. In deriving Eq. (11), we assume that the magnetization vector is

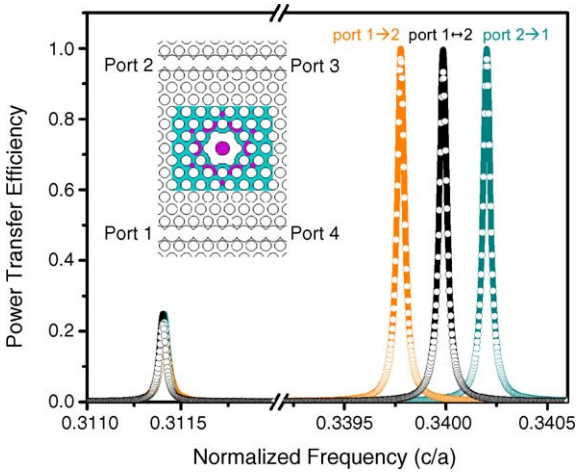

Fig. 3. A comparison of transfer efficiency spectra for an add/drop filter structure with (black) or without magneto-optical coupling (yellow and green). The filter structure is shown in the inset, with the magenta and cyan regions representing magnetization along positive and negative out-of-plane directions. The strength of the magnetization corresponds to an off-diagonal dielectric element $\varepsilon_a = 0.06$. The photonic crystal cavity is constructed with the parameters shown in Fig. 2 and the two waveguides are each constructed by having one row of air holes with an enlarged radius of $0.55a$. The circles and lines correspond to the power transfer coefficients calculated with a finite difference time-domain scheme and the coupled-mode theory, respectively.

along $\hat{\mathbf{z}}$ direction and ε_a takes on positive values when $\hat{\mathbf{z}}$ and the magnetization vector are parallel. Since the states $|e\rangle$and $|o\rangle$ are both standing-wave modes with real-valued electromagnetic fields, the coupling constant between them is purely imaginary, a fact that we previously exploited in Eq. (9).

To create a strong magneto-optical coupling, we note that the electric fields of the defect modes are in-plane and thus the cross product $\vec{E}_o^*(\vec{r}) \times \vec{E}_e(\vec{r})$ lies in the $\hat{\mathbf{z}}$ direction. Since the cross product changes sign rapidly in the cavity, as illustrated in Fig. 2c, it is necessary to have magnetic domains magnetized along opposite directions in various areas of the cavity. The domain structure that maximally couples the two modes $|e\rangle$ and $|o\rangle$ is shown in Fig. 2d. For a constant $|\varepsilon_a|$ in the entire cavity region, the maximum $|\mathbf{V}_{eo}|$ obtained with such domain structure is $0.0213|\varepsilon_a|\omega_o$. In practice, in magneto-optical devices, magnetic domains less than 100 nm can be prepared, [18] which represents a length scale sufficient for photonic crystals operating at 1.55 μm.

The nonreciprocal ADFs, in the strong coupling regime $|\kappa| \gg \gamma$, constitute an ideal four-port circulator. To demonstrate the effect of magneto-optical coupling on the transport properties of photons we choose $|\varepsilon_a| = 0.06$ [19] with the sign of ε_a determined by the magnetic-domain pattern shown as the color patches in the inset of Fig. 3. The power transfer peaks from port 1 to 2 and from port 2 to 1 now shift towards different ends of the spectrum, at frequencies of $\omega_+ = 0.33978(2\pi/a)$ and $\omega_- = 0.34020(2\pi c/a)$ respectively. (Fig. 3) Such nonreciprocal transport is illustrated in Fig. 4, where snapshots of the magnetic field distribution are shown under different excitation conditions. At frequency $\omega = \omega_+$, waves entering port 1

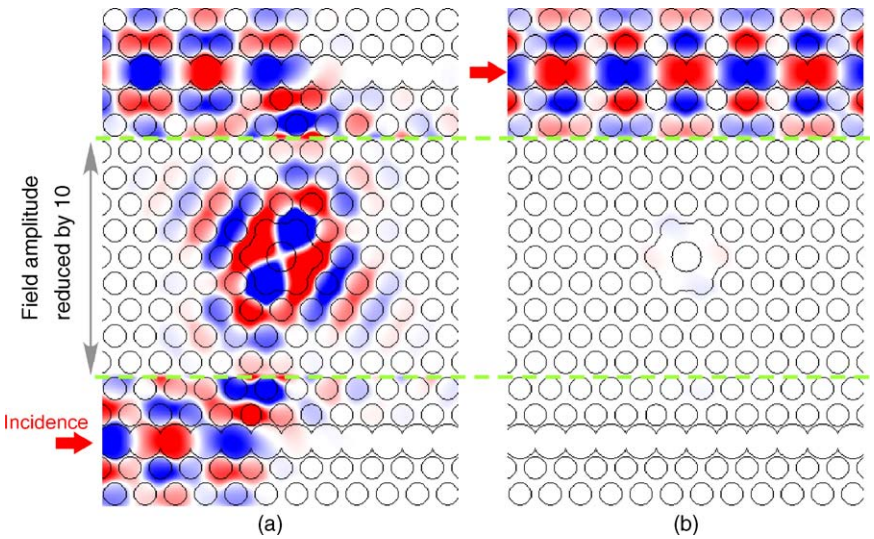

Fig. 4. Snapshots of magnetic fields of the ideal magnetized four-port ADF detailed in Fig. 3. Nonreciprocal transport can be observed when the structure is excited at a frequency of 0.33988 (c/a) from port 1 (a) and port 2 (b). The red and blue colors represent large positive and negative values along out-of-plane directions.

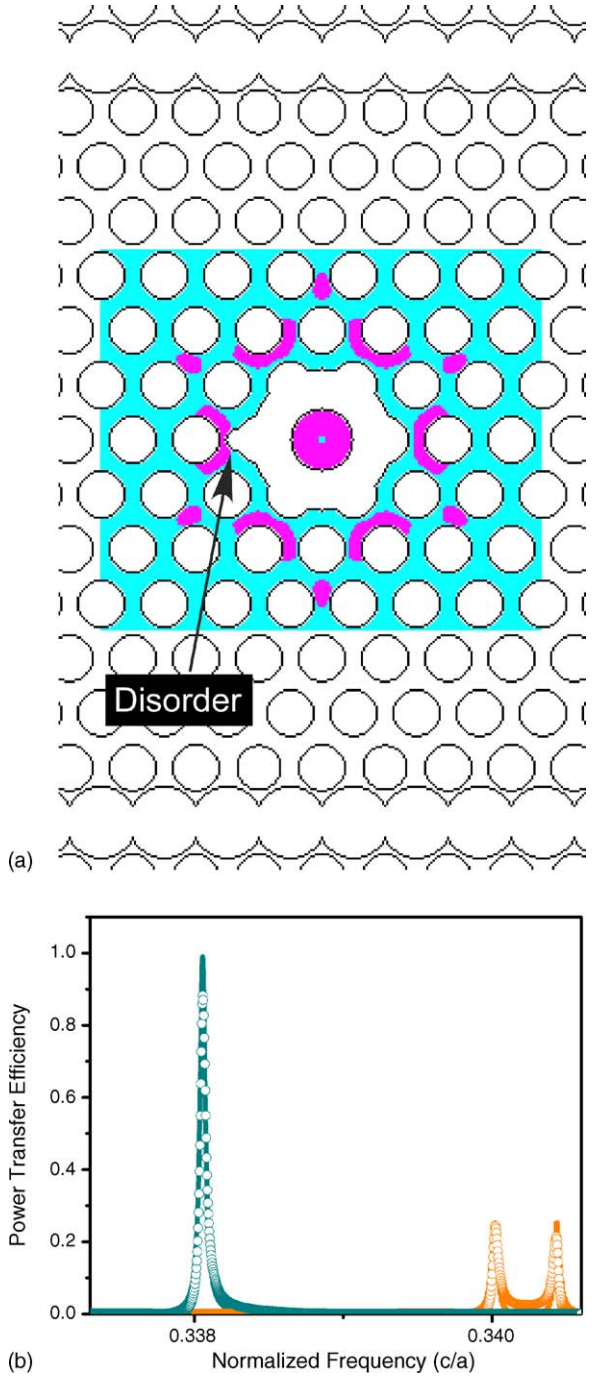

Fig. 5. Transfer efficiency in a non-ideal ADF structure. The structure, shown in (a), is identical to the structure in Fig. 3 inset, except for a large indentation of a radius of $0.15a$ on the outer air ring. The transfer efficiency spectra, with (without) magneto-optical coupling, is shown as a green (orange) curve in (b). The magneto-optical coupling is introduced by assuming $\varepsilon_a = 0.8$ in the colored regions in (a).

tunnel through the resonator and exit at port 2. In contrast, waves entering port 2 exit at port 3, because the detuning between ω_+ and ω_- far exceeds the resonance line width. At frequency ω_+, the transmission characteristics of such circulator is summarized as a 100% clockwise transfer between all ports (i.e.$T_{1\to2} = T_{2\to3} = T_{3\to4} = T_{4\to1} = 1$) and a strongly suppressed counter-clockwise transfer (i.e. $T_{2\to1} = T_{3\to2} = T_{4\to3} = T_{1\to4} \sim -26$ dB). At frequency $\omega = \omega_-$, the opposite transfer characteristics is observed, with the counter-clockwise transfer allowed and the clockwise transfer suppressed. In the design as shown in Fig. 3, a 26 dB contrast ratio between the transfers along opposite directions is maintained near ω_+ and ω_-.

We also note that the transport properties for the modes with other symmetries remain reciprocal. For example, the same point defect structure in this crystal, in the absence of magneto-optical effects, supports a singly degenerate state at $0.31140(2\pi c/a)$. When magneto-optical materials are present, the transport properties remain reciprocal, with a 25% peak transfer efficiency (Fig. 3). In general, the optimized domain structures are selective in creating non-reciprocal coupling only between the chosen mode pair. For in-plane photon transport in photonic crystals, without the correct domain structure non-reciprocal effects cannot be seen in most cases.

To show that magneto-optical coupling can indeed mitigate the effects of degeneracy-breaking perturbations, we now introduce as a disorder an additional semi-circular indentation of a radius of $0.15a$ on the left outer wall of the air ring. (Fig. 5a) In the absence of magneto-optical coupling, this disorder is strong enough to split the nearly 100% transfer peak into two smaller peaks each with only 25% efficiency, and thus completely destroys the ideal channel add/drop characteristics. On the other hand, by applying a strong DC magnetic field ($|\varepsilon_a| = 0.8$), a single peak transfer is restored with the peak efficiency exceeds 90%, as shown in Fig. 5b. Here the FDTD calculation contains higher-order effects and generates slightly lower peak transfer efficiency than the analytical coupled-mode theory, where only the first-order perturbation is considered. Nevertheless, the simulations clearly demonstrate that the effect of disorders is strongly suppressed when the time-reversal symmetry is broken. The circulator operation is robust against small structural perturbations.

5. Discussions

While the simulations here are performed in two-dimensional systems, the operating principles, as

described by coupled-mode theories, can be readily applied to three-dimensional structures including photonic crystal slabs and three-dimensional crystals. Photonic crystal slabs exhibit modal field distribution and dispersion property similar to two-dimensional photonic crystals, [20,21] which implies domain pattern optimized for two-dimensional crystal can also induce strong magneto-optical coupling in similar slab structures. The out-of-plane radiation loss can be reduced to an insignificant level, through the use of ultra-high Q cavities design in 2D slab structures or the use of a three-dimensional photonic crystal cladding [11,22–24]. In both cases, the radiation quality factors (on the order of 10^6) well exceed the waveguide coupling quality factor required in this paper and consequently can be ignored in the coupled-mode analysis.

From the coupled-mode theory, we note that the magneto-optical coupling constants required in the strong coupling regime are directly related to the resonance linewidth. Such large magnetic coupling should be readily achieved in the high Q resonators. Also, to reach strong coupling, instead of using a complex domain structure, one could infiltrate a high-index photonic crystal with a single-domain iron garnet structure with an appropriate size as discussed in Ref [17,25,26]. The maximum magneto-optical coupling is reduced to 50% due to a smaller spatial overlap between the magnetic material with the modal fields. However, uniform external bias can be applied and nanometer-precision domain fabrication can be avoided.

In practice, strong gyrotropy is available in Bi:YIG thin films under an external magnetic bias on the order of 1.6 kOe, with $|\varepsilon_a|$ saturated at 0.06, when operating at 633 nm [19,27,28]. In such strong coupling regime, with the scaling relation and FDTD calculations, the corresponding strength of magneto-optical coupling can restore the complete transfer in the four-port circulator with an indentation of size $0.1a$ similar to Fig. 5a. For an operational wavelength at 1550 nm, this roughness level is equivalent to an indentation on the order of 50 nm.

In certain cases, fabrication imperfections can also strongly affect waveguide-cavity coupling, resulting in a broken degeneracy between the decay rates of the resonances. The effects of such imperfections cannot be suppressed by the nonreciprocal coupling considered here and would have to be corrected with post-fabrication trimming. Moreover, surface roughness may still contribute to an overall drift of the resonance frequencies. Consequently, to have a precise resonant wavelength that aligns with a particular channel, it may still require active tuning of the device. For the magneto-optical effects considered here, this can be accomplished, for example, by varying the strength of the external DC magnetic bias to control the related resonance frequency.

Acknowledgements

We acknowledge the support of a Packard Fellowship in Science and Engineering. The simulations were made possible by the IBM-SUR program and a NSF-NRAC grant.

References

[1] S. John, Strong localization of photons in certain disordered dielectric superlattices, Phys. Rev. Lett. 58 (1987) 2486–2489.
[2] E. Yablonovitch, Inhibited spontaneous emission in solid-state physics and electronics, Phys. Rev. Lett. 58 (1987) 2059–2062.
[3] J.D. Joannopoulos, R.D. Meade, J.N. Winn, Photonic Crystals: Molding the Flow of Light, Princeton University Press, Princeton, N.J, 1995.
[4] M. Inoue, K. Arai, T. Fujii, M. Abe, Magneto-optical properties of one-dimensional photonic crystals composed of magnetic and dielectric layers, J. Appl. Phys. 83 (1998) 6768–6770.
[5] M.J. Steel, M. Levy, R.M. Osgood, High transmission enhanced Faraday rotation in one-dimensional photonic crystals with defects, IEEE Photon. Technol. Lett. 12 (2000) 1171–1173.
[6] I.L. Lyubchanskii, N.N. Dadoenkova, M.I. Lyubchanskii, E.A. Shapovalov, T.H. Rasing, Magnetic photonic crystals., J. Phys. D Appl. Phys. 36 (2003) R277–R287.
[7] B.E.A. Saleh, M.C. Teich, Fundamentals of Photonics, Wiley, New York, 1991.
[8] S. Fan, P.R. Villeneuve, J.D. Joannopoulos, H.A. Haus, Channel drop tunneling through localized states, Phys. Rev. Lett. 80 (1998) 960–963.
[9] S. Fan, P.R. Villeneuve, J.D. Joannopoulos, Channel drop filters in photonic crystals, Opt. Express 3 (1998) 4–11.
[10] S. Noda, T. Baba, Optoelectronic Industry Technology Development Association (Japan), Roadmap on photonic crystals, Kluwer Academic Publishers, Dordrecht; Boston, 2003.
[11] H. Takano, B.S. Song, T. Asano, S. Noda, Highly efficient in-plane channel drop filter in a two-dimensional heterophotonic crystal, Appl. Phys. Lett. (USA) 86 (2005) 241101–241102.
[12] H.A. Haus, W.P. Huang, Coupled-mode theory, Proc. IEEE 79 (1991) 1505–1518.
[13] C. Manolatou, M.J. Khan, S.H. Fan, P.R. Villeneuve, H.A. Haus, J.D. Joannopoulos, Coupling of modes analysis of resonant channel add-drop filters, IEEE J. Quan. Electron. 35 (1999) 1322–1331.
[14] W. Suh, Z. Wang, S. Fan, Temporal coupled-mode theory and the presence of non-orthogonal modes in lossless multimode cavities, IEEE J. Quan. Electron. 40 (2004) 1511–1518.
[15] Y. Xu, Y. Li, R.K. Lee, A. Yariv, Scattering-theory analysis of waveguide-resonator coupling, Phys. Rev. E: Stat. Phys., Plasma, Fluids 62 (2000) 7389–7404.
[16] Z. Wang, S.F. Fan, Optical circulators in two-dimensional magneto-optical photonic crystals, Optics Lett. 30 (2005) 1989–1991.

[17] Z. Wang, S. Fan, Magneto-optical defects in two-dimensional photonic crystals, Appl. Phys. B: Lasers Opt. 81 (2005) 369–375.

[18] Z. Deng, E. Yenilmez, J. Leu, J.E. Hoffman, E.W.J. Straver, H. Dai, K.A. Moler, Metal-coated carbon nanotube tips for magnetic force microscopy, Appl. Phys. Lett. 85 (2004) 6263–6265.

[19] N. Adachi, V.P. Denysenkov, S.I. Khartsev, A.M. Grishin, T. Okuda, Epitaxial $Bi_3Fe_5O_{12}$(0 0 1) films grown by pulsed laser deposition and reactive ion beam sputtering techniques, J. Appl. Phys. 88 (2000) 2734–2739.

[20] S.G. Johnson, F. Shanhui, P.R. Villeneuve, J.D. Joannopoulos, L.A. Kolodziejski, Guided modes in photonic crystal slabs, Phys. Rev. B 60 (1999) 5751–5758.

[21] M. Qiu, Effective index method for heterostructure-slab-waveguide-based two-dimensional photonic crystals, Appl. Phys. Lett. 81 (2002) 1163–1165.

[22] B.-S. Song, S. Noda, T. Asano, Y. Akahane, Ultra-high-Q photonic double-heterostructure nanocavity, Nat. Mater. 4 (2005) 207–210.

[23] M.L. Povinelli, S.G. Johnson, S. Fan, J.D. Joannopoulos, Emulation of two-dimensional photonic crystal defect modes in a photonic crystal with a three-dimensional photonic band gap., Phys. Rev. B Condens. Matter Mater. Phys. 64 (2001) 075313–075318.

[24] H. Takano, Y. Akahane, T. Asano, S. Noda, In-plane-type channel drop filter in a two-dimensional photonic crystal slab, Appl. Phys. Lett. 84 (2004) 2226–2228.

[25] T. Kodama, K. Nishimura, A.V. Baryshev, H. Uchida, M. Inoue, Opal photonic crystals impregnated with magnetite, Phys. Status Solidi B 241 (2004) 1597–1600.

[26] T. Ishibashi, A. Mizusawa, M. Nagai, S. Shimizu, K. Sato, N. Togashi, T. Mogi, M. Houchido, H. Sano, K. Kuriyama, Characterization of epitaxial (Y,Bi){sub 3}(Fe,Ga){sub 5}O{sub 12} thin films grown by metal-organic decomposition method, J. Appl. Phys. 97 (2005) 13516–13521.

[27] T.M. Le, F. Huang, D.D. Stancil, D.N. Lambeth, Bismuth substituted iron garnet thin films deposited on silicon by laser ablation, J. Appl. Phys. 77 (1995) 2128–2132.

[28] T. Tepper, C.A. Ross, Pulsed laser deposition and refractive index measurement of fully substituted bismuth iron garnet films., J. Cryst. Growth 255 (2003) 324–331.

[29] S.G. Johnson, J.D. Joannopoulos, Block-iterative frequency-domain methods for Maxwell's equations in a planewave basis, Opt. Express 8 (2001) 173–190.